ACSNANO

www.acsnano.org

ARTICLE

Mechanistic Study for Facile Electrochemical Patterning of Surfaces with Metal Oxides

Evan C. Jones,[†] Qihan Liu,[‡] Zhigang Suo,[*,‡] and Daniel G. Nocera[*,†]

[†]Department of Chemistry and Chemical Biology and [‡]John A. Paulson School of Engineering and Applied Sciences, Harvard University, Cambridge, Massachusetts 02138, United States

Supporting Information

ABSTRACT: **Reactive interface patterning promoted by lithographic electrochemistry serves as a method for generating submicrometer scale structures. We use a binary-potential step on a metallic overlayer on silicon to fabricate radial patterns of cobalt oxide on the nanoscale. The mechanism for pattern formation has heretofore been ill-defined. The binary potential step allows the electrochemical boundary conditions to be controlled such that initial conditions for a scaling analysis are afforded. With the use of the scaling analysis, a mechanism for producing the observed pattern geometry is correlated to the sequence of electrochemical steps involved in the formation of the submicrometer structures. The patterning method is facile and adds to electrochemical micromachining techniques employing a silicon substrate.**

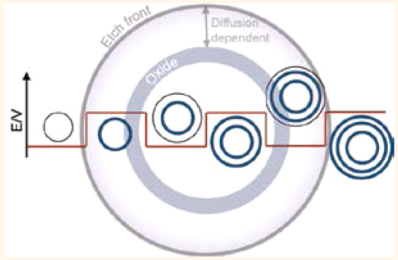

KEYWORDS: *electrochemical micromachining, nanopattern, silicon, oxide catalysts, finite element simulation*

Electrochemical micromachining (EMM) involves shaping materials on the micrometer to submicrometer scale by performing electrochemistry, conventionally through small openings in an insulating mask.[1,2] The benefits of EMM include exceptional control of etching rate and extent, as well as an ability to smoothly shape conductive materials of any hardness and domain size without incurring wear.[3−6] However, EMM has traditionally been limited to the removal of material, restricting the technique to precision milling. We have recently reported an EMM method designated RIPPLE (reactive interface patterning promoted by lithographic electrochemistry), which entails electrochemically patterning thin films of metal (*e.g.*, cobalt, copper) or semimetal (germanium) on silicon by way of cyclic voltammetry (CV).[7] Well-defined patterning has been elucidated as a function of applied potential and scan rate. In using cyclic voltammetry to generate patterns, linearly scanning across a voltage window induces varying fluxes and also potentially introduces unnecessary processes or intermediates within each scan. These complexities, which present challenges to defining the mechanism of RIPPLE, are mitigated by toggling between the potential limits of the cyclic voltammetry experiment with a binary potential step method. Using such a voltage profile allows us to provide robust initial conditions for a scaling analysis. Comparison of observed patterns to those predicted by the scaling analysis furnishes insight into the mechanism of patterning by RIPPLE.

RESULTS AND DISCUSSION

A binary-potential step method, schematically shown in Figure S1, was used to generate patterns from cobalt overlaid on silicon by alternating between two discrete potentials. These experiments were conducted with p-doped silicon substrates coated with a 250 nm cobalt film, which was masked by poly(methyl methacrylate) (PMMA) e-beam resist, as previously described.[7] The mask contains a 9 × 9 array of 4 μm^2 square openings. The sample was suspended in 0.1 M K_2SO_4 and subjected to 10 potential steps (all potentials are reported *vs* Ag/AgCl) of 0.4 V (applied for 10 s) and 1.3 V (applied for 3 s), which correspond to the CV scan limits previously used to pattern silicon with cobalt oxide by RIPPLE.[7] As shown in Figure 1, concentric rings are produced. Atomic force microscopy (AFM) shows that the ridges are 1.4 μm wide and 130 nm tall. Scanning electron microscopy (SEM) with energy X-ray dispersion spectroscopy maps of Co and O indicates that the ridges are composed of Co oxide. The gaps between the rings and ring thicknesses are attenuated as a function of distance from the pattern's center. The rings generated by the binary-potential step are comparable to those by the CV-based RIPPLE method with regard to both ring definition and spacing (Figure S2).

By modulating the durations of the 0.4 and 1.3 V steps, the spacing between rings and the ring widths could be adjusted, respectively (Figure S3). The correlation between ring spacings and ring widths with their respective potentials implies that at 0.4 V, the etching of Co metal occurs, while at 1.3 V, an oxide layer is formed. This result suggests that potential steps could be programmed to control the geometries of the metal oxide pattern. To demonstrate this correlation, patterns with

Received: February 22, 2016
Accepted: April 11, 2016
Published: April 13, 2016

DOI: 10.1021/acsnano.6b01335
ACS Nano 2016, 10, 5321−5325

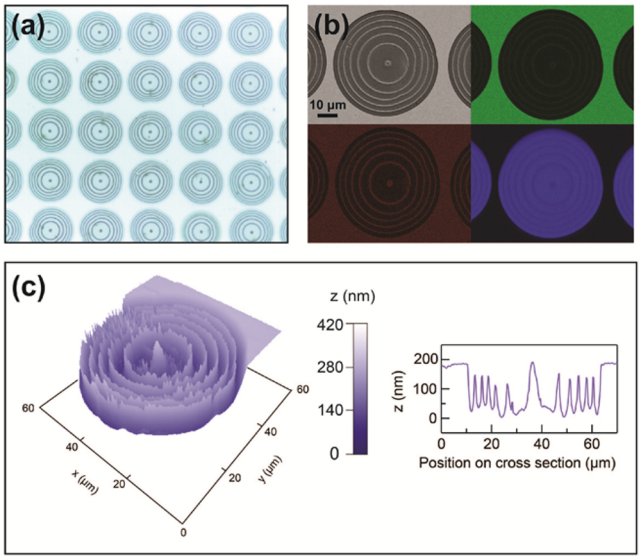

Figure 1. Patterns formed by alternating between 0.4 V (10 s) and 1.3 V (3 s) 10 times in 0.1 M K_2SO_4. (a) Optical microscope images at 50× magnification. (b) SEM image (*top left*) and EDS elemental maps of cobalt (green), oxygen (red), and silicon (blue). (c) AFM map with height-profile of a diametric cross section (*inset on right*).

uniformed gap and ring dimensions were formed by sequentially increasing the duration of each step to compensate for the decreasing spacing between rings. For example, the well-defined pattern of rings of 3.0 μm width and 3.8 μm spacing shown in Figure 2 was generated for binary potential steps held for 5, 7, 9, 12, and 15 s.

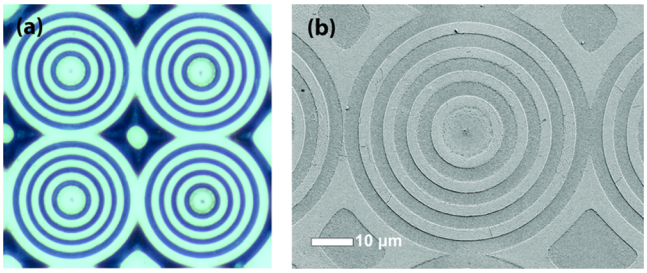

Figure 2. Patterns with conserved radial dimensions formed by sequentially increasing potential step durations in 0.1 M K_2SO_4. Images from (a) optical microscope with 50× objective and (b) SEM.

To delineate the correlation between applied potentials and the patterning process, the pattern was surveyed by *in situ* optical microscopy. A video recording of the pattern formation by alternating between 0.4 V (10 s) and 1.3 V (3 s) 10 times was synchronized to the applied potential and current so that the evolution of a pattern could be observed through optical micrographs (Figure S4). A bright-contrasted circle expands from the opening for the first 10 s, followed by 3 s upon which a dark-contrast ring propagates into the surrounding area. From AFM height and EDS maps (Figure 1b,c), it was determined that the bright-contrasted circle and surrounding bright-contrast rings correspond to regions where cobalt was removed and the dark-contrasted rings correspond to cobalt oxide. These results are in agreement with the assignment to an etching process at 0.4 V and metal oxide formation at 1.3 V.

With consideration to the Pourbaix diagram of Co, the reaction during etching at 0.4 V in 0.1 M K_2SO_4 corresponds to the two-electron oxidation of Co^0 to a soluble Co^{2+} ion or $CoO(OH)^-$.[8] Similar diameters of the etch fronts after stepping the potential to 0.2, 0.3, and 0.4 V for 10 s (Figure S5) indicate that the etching rate is not limited by the applied voltage. Optical microscopy, SEM and EDS show that an oxide layer formed after a delay is identical to applying 1.3 V successively after etching (Figure S6). Therefore, the oxide formation process is independent of diffusion, suggesting that the primary pathway for oxide formation is the direct conversion of Co metal to Co oxide. Cobalt is thus etched away at 0.4 V and the metallic front at the boundary of the etching front is converted into the oxide ridge at 1.3 V by the reaction of Co metal with water under this anodic potential. This is consistent with the observation that the oxide layer extends into the Co^0 film during application of 1.3 V (Figure S4). The next ring is then formed upon cobalt etching from the backside of the Co oxide ring. The Co^{2+} ions produced during etching diffuse over the top of rings to the opening in the mask.

The kinetics process of Co^{2+} diffusion from the etch front is explored with finite element simulations. Defining c as the concentration and J as the flux of Co^{2+}, the conservation of Co^{2+} requires that

$$\frac{\partial c}{\partial t} = -\nabla \cdot \mathbf{J} \tag{1}$$

The simplest case is for $\mathbf{J}$ to obey Fick's law,

$$\mathbf{J} = -D\nabla c \tag{2}$$

Dimensional analysis of eqs 1 and 2 furnishes a relaxation time,

$$t \sim \frac{L^2}{D} \tag{3}$$

where t is the relaxation time, L is the distance from the etching front to the opening, which should be on the order of 10 μm, and D is the diffusivity. Co^{2+} ions are expected to have a diffusion coefficient close to the self-diffusivity of water, on order of 10^{-9} m^2/s.[9] Equation 3 furnishes a relaxation time on the order of 0.1 s, which is much shorter than the time scale of operation at 0.4 V (10 s). Consequently, diffusion is taken to be at steady state during etching and the left-hand side of eq 1 is equal to zero. Under these assumptions, the etching rate at any time can be calculated.

At the etch front, we assume the concentration of the Co^{2+} is limited by a saturated value c_{sat}, which gives one boundary condition,

$$c|_{front} = c_{sat} \tag{4}$$

The concentration of Co^{2+} is assumed to be 0 M at the opening, which gives the other boundary condition,

$$c|_{opening} = 0 \tag{5}$$

Equations 1, 2, 4, and 5, under the steady state assumption, constitute a complete boundary value problem that uniquely determines the concentration distribution once the size of the opening and the position of the etching front are prescribed. The etching front moves as metallic Co is etched. The normal velocity of the etching front is

$$v_n = J\Omega \tag{6}$$

DOI: 10.1021/acsnano.6b01335
ACS Nano 2016, 10, 5321−5325

where Ω is the molar volume of the metallic Co and J is the magnitude of the diffusion flux, which is always perpendicular to the etch front due to eq 4. In the axisymmetric case, an analytical solution for eqs 1, 2, 4, and 5 exists,

$$c(r) = c_{sat}\frac{\ln r - \ln r_0}{\ln r_f - \ln r_0} \tag{7}$$

where r_0 and r_f denote the position of the edge of the opening and the etching front. Correspondingly, if we combine eqs 2 and 6 and compute ∇c from eq 7, the velocity of the etch front is

$$\nu_n = \frac{Dc_{sat}\Omega}{\ln r_f - \ln r_0}\frac{1}{r_f} \tag{8}$$

By definition, $\nu_n = dr_f/dt$. The time evolution of r_f can be numerically integrated based on eq 8. Figure 3 is calculated in this way, where blue lines denote the position of the etching front after every 10 s of etching. In this simulation, we assume that the thickness of the oxide rings is much smaller than the distance between the rings and that the rings do not markedly affect the kinetics of diffusion. With regard to the latter, the diffusion is not significantly affected if the spacing over the top of the ring is more than ~1/10 the height of the film thickness (*i.e.*, the spacing between the Si substrate and the mask overlayer). Figure 1c shows that this condition is met. The average ring height is 123 nm *vs* a film thickness of 173 nm, and thus, the average difference in ring height from film thickness is 50 nm, or approximately 30% of the film thickness. In addition, the Co oxide ring is porous and fluid may flow through the oxide ring. Hence, the presence of rings does not greatly perturb diffusion for the purposes of this model. The blue rings shown in Figure 3 correspond to the position of oxide rings observed in experiments. In the calculation of Figure 3, the opening size is chosen as r_0 = 1 μm. The molar volume of metallic Co is Ω = 6.6 mL/mol, and we take c_{sat} = 1 M, which is approximately the solubility of saturated $CoSO_4$ solution. The initial condition (t = 0) for the calculation is $r_f = r_0$ + 0.1 μm.

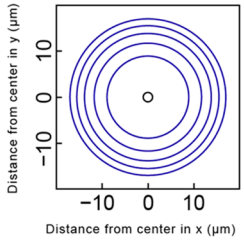

Figure 3. Predicted ring spacing from finite-element simulations. Ring positions (blue) relative to a 1 μm-diameter circular opening (black). Note ring spacing decreases with increasing distance from the opening.

Whereas the concentration of Co^{2+} at the opening was set to 0 M in furnishing the results of Figure 3, a nonvanishing concentration is required to drive the diffusion from the opening to the bulk electrolyte (Figure S7a). The space under the resist is highly confined compared to the space outside the opening, and therefore, we expect a much steeper concentration gradient from the etch front to the opening as compared to from the opening to the bulk electrolyte. Consequently, no matter what the concentration at the opening may be, it will always be small compared to the concentration at the etch front. Thus, setting $c|_{opening}$ = 0 M as a boundary condition does not significantly change the diffusion rate. We note that $c|_{front}$ = 1 M is much higher than the concentration of the supporting electrolyte, 0.1 M. The complete expression of flux should thus account for the contribution from migration due to this difference in ionic strength,

$$\mathbf{J} = -D\nabla c - \frac{ze}{kT}D\nabla c\phi \tag{9}$$

where z is the valence of Co^{2+} and ϕ is the electric potential. The fluxes of the other two ions, SO_4^{2-} and K^+, satisfy similar relations, with their own concentrations and diffusivities. Outside the double layer from the boundary, the solution is electrically neutral. Consequently, the electric potential satisfies the Laplace equation,

$$\nabla^2\phi = 0 \tag{10}$$

Whereas the electric field couples the fluxes of the three species of ions, a simple decoupled approximation exists. At steady state, the total flux of SO_4^{2-} vanishes, so that the flux of SO_4^{2-} due to migration exactly balances that due to diffusion. Because the concentration of Co^{2+} is high, the concentration of K^+ is negligible. Accordingly, to maintain electroneutrality, the concentration of SO_4^{2-} nearly equals the concentration of Co^{2+}. Note that Co^{2+} and SO_4^{2-} carry charges of the opposite valences. Consequently, the migration flux of Co^{2+} also equals its diffusion flux in magnitude, but the two fluxes are in the same direction. In this case, the modeling accounted for by eq 2 remains valid by doubling the value of the diffusivity,

$$\mathbf{J} = -2D\nabla c \tag{11}$$

It is worth noting that Figure S7b, which was generated by a finite element simulation using COMSOL software, shows that the concentration of Co^{2+} at the opening is about an order of magnitude lower than its concentration at the etching front. It also shows that the concentration of K^+ is very low so that the concentration of SO_4^{2-} roughly equals the concentration of Co^{2+}. These serve to validate the above approximations to yield eqs 5 and 11.

The model for RIPPLE is etching metallic Co at low anodic potentials followed by oxidation of the metal to Co oxide when the potential is stepped to more positive anodic potential. Upon returning the potential, Co oxide formation ceases, and etching begins on the backside of the Co oxide ring, extending away from the center of the ring. Our analysis indicates that the etching process is dictated by cobalt ion diffusion upon etching. The analysis illustrates that as the etch front of metallic Co progresses from the opening, the mass transport of Co^{2+} away from the etch front is deterred because the distance for diffusion into bulk electrolyte increases. Since the concentration at the etching front is limited by the saturated concentration of Co^{2+} and the concentration at the opening is effectively zero, the increase in distance results in a decrease in concentration gradient, which results in a lower diffusion flux. The lower diffusion flux corresponds to slower etching further from the center of the pattern, which accounts for the decreasing ring spacing in the experimental results observed in Figure 1. It should also be mentioned that for the simulation of the pattern, we only consider the spacing between the rings. The presence of oxide rings is expected to further narrow the spacing by constricting the diffusion path. However, the geometries of the rings are not critical for observing the trend in the ring spacing. This trend in ring spacing is verified experimentally (Figure 1).

DOI: 10.1021/acsnano.6b01335
ACS Nano 2016, 10, 5321−5325

Our experimental results supported by analysis show that the mechanism of pattern formation by RIPPLE establishes that the ring position depends on the distance of cobalt ion diffusion into bulk electrolyte, with the kinetics limited by the diffusion of Co^{2+} from the etching front to the opening.

CONCLUSIONS

Radial patterns of Co oxide are formed in 0.1 M K_2SO_4 by first oxidizing Co^0 to Co^{2+} at 0.4 V, which results in etching from the opening in the mask to the inner radius of the first ring. The resulting metal perimeter is then directly oxidized to Co oxide at 1.3 V to form the ring. Ring spacings and widths may be adjusted by modulating the duration of the 0.4 and 1.3 V potential steps, respectively. By partitioning the patterning process into two discrete potential steps, we achieve improved control of pattern geometry and boundary conditions for the patterning process may be controlled. With the use of the scaling analysis, a mechanism for producing the observed pattern geometry is correlated to the sequence of electrochemical steps involved in the formation of the submicrometer structures, thus allowing for precise control of the pattern geometry. The ability to pattern large areas of silicon periodically with submicrometer inorganic oxides affords a facile method for electrochemically integrating materials with silicon.

METHODS

Materials. Co metal pellets ($^1/_8$ in. × $^1/_8$ in. dia., 99.95%, Kurt J. Lesker), K_2SO_4 (99.0% min, Alfa Aesar), 950PMMA C4 (MicroChem), stop-off lacquer (MICCRO Products), 1:3 methyl isobutyl ketone/isopropyl alcohol (MIBK/IPA) developer (MicroChem), IPA (99.5%, Sigma-Aldrich), and acetone (99%, Sigma-Aldrich) were used as received. Four inch, p-type Si wafers (B-doped, ⟨ 100⟩, 1−10 Ω·cm, Nova Electronic Materials) were etched in 7:1 buffered oxide etch (BOE, J.T. Baker) and rinsed with water 30 s immediately before use. Type I water (EMD Millipore, 18.2 MΩ·cm) was used to prepare solutions. The pH of 0.1 M K_2SO_4 solution was unadjusted (measured as pH 8.4).

Working Electrode Fabrication. The working electrode to be patterned was fabricated by loading a recently etched p-type Si 4 in. wafer and a crucible of Co metal pellets into the chamber of a Sharon electron beam vapor deposition system. The chamber was evacuated to 1 μTorr. The crucible was gradually heated over 1 h by slowly increasing the current until it reached 60 mA at 10 kV. A shutter was manually opened to allow the growth of a 250 nm Co film on the p-Si, while monitoring film growth with a piezoelectric quartz crystal.

The electrode surface was masked by spin-coating 950PMMA C4 resist over the Co film at 4000 rpm for 45 s and then heating the substrate to 185 °C over 4 min. An electron-beam writer (JEOL-7000) was used to define a square 9 × 9 array of 2 μm × 2 μm square openings in the PMMA. The openings were spaced 80 μm from the nearest neighbor. The PMMA was developed for 45 s in 1:3 MIBK/IPA developer and soaked in IPA for 45 s. Resist thickness and opening dimensions were confirmed by AFM. The back of the sample (p-Si) and the sample edges were coated with lacquer.

General Electrochemical Methods. All electrochemical experiments were conducted using a CH Instruments 760D bipotentiostat, a Pt-mesh counter electrode, and a BASi Ag/AgCl reference electrode (stored in saturated KCl), except for *in situ* microscopy, which utilized either a microreference electrode (none-leak interface, Innovative Instruments) or a BASi Ag/AgCl reference electrode encased in a Luggin capillary tube fabricated by stretching a glass pipet over a flame. All electrochemical experiments were performed with a three-electrode setup within a plastic beaker, except for the *in situ* recording, where the working electrode was laid horizontal and 0.1 M K_2SO_4 was dropped onto the surface. A microreference electrode and Pt wire were inserted into the drop, which was contained on the electrode by surface tension. All procedures were performed at ambient temperature (23 ± 1 °C). The microreference electrode contained 3.4 M KCl and was corrected to match the saturated KCl solution using E(Ag/AgCl sat. KCl) = E(Ag/AgCl 3.4 M KCl) + 0.035 V (measured). All potentials mentioned are referenced to Ag/AgCl (saturated KCl).

Consistently wide rings and gaps were generated with the following potential steps in their respective order: 0.4 V (5 s), 1.3 V (5 s), 0.4 V (7 s), 1.3 V (7 s), 0.4 V (9 s), 1.3 V (9 s), 0.4 V (12 s), 1.3 V (12 s), 0.4 V (15 s), 1.3 V (15 s), 0.4 V (20 s).

Microscopy. Optical microscopy was performed using an Axio Scope.A1 microscope in conjunction with 20× and 50× objectives, a 63× water immersion objective, and an AxioCam ICc 5 (all components Carl Zeiss Microscopy).

Field emission SEM was performed with a Zeiss Supra55VP. The SEM was operated at 3 kV at a working distance of *ca.* 8 mm with a 30 μm aperture and used the secondary electron (SE2) detector. EDS was performed with an EDAX detector at an electron-beam voltage of 14 kV. The EDS maps were acquired with a dwell time of 200 ms, a resolution of 1024 × 800, and at a working distance of 8.5 mm.

AFM was conducted with AC mode using an MFP-3D system (Asylum Research) with a 300 kHz Al-coated Si AFM tip (Asylum Research) with a scan rate of 0.3 or 0.6 kHz. The AFM maps were masked, flattened, filtered, and line erased for clarity. The "Dull Yellow" color scheme was applied and set to inverted and negative color.

ASSOCIATED CONTENT

Supporting Information

The Supporting Information is available free of charge on the ACS Publications website at DOI: 10.1021/acsnano.6b01335.

Additional experimental data (Figures S1−S7) (PDF)

AUTHOR INFORMATION

Corresponding Authors

*E-mail: dnocera@fas.harvard.edu.
*E-mail: suo@seas.harvard.edu.

Notes

The authors declare no competing financial interest.

ACKNOWLEDGMENTS

J. Tresback is thanked for assistance in conducting AFM experiments. Support of this work by NSF CCI Center CHE-1305124 (D.G.N.) and NSF MRSEC DMR 14-20570 (Z.S.) is gratefully acknowledged. E.C.J. gratefully acknowledges the National Science Foundation (NSF) for a predoctoral fellowship. This work was performed in part at the Center for Nanoscale Systems, part of Harvard University and a member of the National Nanotechnology Infrastructure Network, which is supported by NSF under Award No. ECS-0335765.

REFERENCES

(1) Köhler, M. *Etching in Microsystem Technology*; Wiegand, A., Transl.; Wiley-VCH: Weinheim, Germany, 1999; pp 74−79.

(2) Kern, P.; Veh, J.; Michler, J. New Developments In Through-Mask Electrochemical Micromachining of Titanium. *J. Micromech. Microeng.* **2007**, *17*, 1168−1177.

(3) Li, W.; Quandai, W.; Xiuqing, H.; Yucheng, D.; Bingheng, L. Finite Element Simulation and Experimental Study on the Through-Mask Electrochemical Micromachining (EMM) Process. *Int. J. Adv. Manuf. Technol.* **2010**, *51*, 155−162.

(4) Schuster, R.; Kirchner, V.; Allongue, P.; Ertl, G. Electrochemical Micromachining. *Science* **2000**, *289*, 98−101.

DOI: 10.1021/acsnano.6b01335
ACS Nano 2016, 10, 5321−5325

(5) Datta, M.; Romankiw, L. T. Application of Chemical and Electrochemical Micromachining in the Electronics Industry. *J. Electrochem. Soc.* **1989**, *136*, 285C−292C.
(6) Datta, M.; Landolt, D. Fundamental Aspects and Applications of Electrochemical Microfabrication. *Electrochim. Acta* **2000**, *45*, 2535−2558.
(7) Kempa, T. J.; Bediako, D. K.; Jones, E. C.; Lieber, C. M.; Nocera, D. G. Facile, Rapid, and Large-Area Periodic Patterning of Semiconductor Substrates with Submicron Inorganic Structures. *J. Am. Chem. Soc.* **2015**, *137*, 3739−3742.
(8) Pourbaix, M. *Atlas of Electrochemical Equilibria in Aqueous Solutions*; Pergamon Press: Oxford, 1966; pp 322−329.
(9) Bard, A. J.; Faulkner, L. R. *Electrochemical Methods: Fundamentals and Applications*, 2nd ed; John Wiley and Sons: New York, 2001; Chapter 4.

DOI: 10.1021/acsnano.6b01335
ACS Nano 2016, 10, 5321−5325